Higher-Order Tensor Independent Component Analysis for MIMO Remote Sensing of Respiration and Heartbeat Signals

Seishiro Goto, *Graduate Student Member, IEEE*, Ryo Natsuaki, *Senior Member, IEEE*, and Akira Hirose, *Fellow, IEEE*

***Abstract*— This paper proposes a novel method of independent component analysis (ICA), which we name higher-order tensor ICA (HOT-ICA). We newly develop a robust microwave multiple-input multiple-output (MIMO) radar system, in which HOT-ICA performs separation of multiple-target signals to detect respiration and heartbeat. In comparison with millimeter waves, microwaves spread wider with diffraction and propagate even in an environment with obstacles to reach targets. However, it often requires more powerful signal separation because of its lower resolution. HOT-ICA realizes high robustness in self-organization of a separation tensor by utilizing channel information, i.e., the information of physical-measurement circumstances concerning, e.g., which transmitting/receiving antennas are used. In numerical and living-human experiments, our HOT-ICA system effectively separates the bio-signals successfully even in an obstacle-affecting environment, which has been a difficult task. The results demonstrate the significance of HOT-ICA in remote sensing. It fully utilizes the high dimensionality of the separation tensor by keeping the tensor structure unchanged to take advantage of the measurement-circumstances information.**

***Index Terms*— Complex-valued neural network, Doppler radar, independent component analysis (ICA), multiple-input multiple-output (MIMO) system.**

I. Introduction

CONVENTIONAL heartbeat and/or respiration sensing systems use contact-type electrodes attached to a human body. However, recent vital-sign detectors sometimes employ noncontact methods. After the first report of detection of respiration using microwaves [1], there have been a lot of research on respiration and heartbeat measurement based on Doppler radar. Some of them assumed line-of-sight (LOS) situations [2], [3], [4], [5], [6], [7], while others worked on non-line-of-sight (NLOS) conditions including search and rescue in disasters such as earthquake rubble [8], [9], [10], [11], [12], [13].

Multiple-input multiple-output (MIMO) configuration using multiple transmitting and receiving antennas holds the ability of target identification intrinsically. For example, a 24 GHz frequency-modulation continuous-wave (FMCW) MIMO radar detects respiration and heartbeat information for respective targets by using target distances to separate the individuals [14]. However, the use of such a high frequency limits its practical applications only within short-range LOS situations. The difficulty is found also in ultrasound sensing systems [15]. A lower-frequency continuous-wave (CW) radar system has the potential to realize target detection with a wider sensitive area even including obstacles.

Environments having obstacles and multiple targets often require separation of a target signal from others and noise. A signal-source separation experiment in an X-band array radar was reported [16], in which the heartbeat signal of one target was separated from that of another one by using beamforming successfully. However, a microwave having a lower frequency possesses an advantage though their spatial resolution is a little lower. Microwaves are capable of propagating among obstructions because of their diffractive nature. In such a case, blind source separation (BSS) is expected to enhance the detection and identification ability.

BSS is a framework to estimate individual original signals included in mixed signals based on signal information itself. Independent component analysis (ICA) is a typical method in BSS [17], [18], [19]. ICA eliminates noise and/or separates targets by finding a separation matrix to linearly transform mixed signals into unmixed ones based on signals' statistical property. ICA has been often employed in audio signal processing in the frequency domain [20], [21], [22].

In the radar sensing and imaging field, an ICA system [11] treated in-phase and the quadrature components obtained by orthogonal detection as two real-number signals different from each other. However, a pair of in-phase and orthogonal components should be processed essentially as a single complex signal [23], [24], [25]. This present paper also deals with complex signals as an entity. In vital sensing, measurement

Manuscript received 11 December 2022; revised 1 March 2023; accepted 13 March 2023. Date of publication 20 March 2023; date of current version 18 April 2023. This work was supported in part by the Japan Society for the Promotion of Science (JSPS) KAKENHI under Grant 18H04105, and in part by the Cooperative Research Project Program of the Research Institute of Electrical Communication (RIEC), Tohoku University. An earlier version of this paper was presented in part at the Annual International Conference of the IEEE Engineering in Medicine Biology Society (EMBC) 2021 [DOI: 10.1109/EMBC46164.2021.9630656]. *(Corresponding author: Seishiro Goto.)*

Seishiro Goto is with the Department of Bioengineering, The University of Tokyo, Tokyo 113-8656, Japan (e-mail: seishiro_goto@eis.t.u-tokyo.ac.jp).

Ryo Natsuaki is with the Department of Electrical Engineering and Information Systems, The University of Tokyo, Tokyo 113-8656, Japan (e-mail: natsuaki@ee.t.u-tokyo.ac.jp).

Akira Hirose is with the Department of Bioengineering and the Department of Electrical Engineering and Information Systems, The University of Tokyo, Tokyo 113-8656, Japan (e-mail: ahirose@ee.t.u-tokyo.ac.jp).

Digital Object Identifier 10.1109/TRS.2023.3259326

environment often varies depending on target movement and obstacles. We thus aim to process complex signals adaptively in time-sequential observation [26], [27]. The scheme is called online ICA.

Signal processing in measurement using MIMO configuration leads to a construction of data tensor having multiple axes involving path-category information, rather than a data vector representing mixed signals evenly. A tensor data requires a higher-order tensor for signal separation. Multilinear ICA (MICA) was proposed for applying third-order tensors to ICA processing [28], [29]. MICA uses higher-order singular value decomposition (HOSVD) or higher-order orthogonal iteration (HOOI) [30], [31], [32]. Their calculation is based on the tensor decomposition proposed by Tucker [33]. MICA has been positively evaluated for its separation effectiveness [34], [35], [36], [37].

Though it is true that the methods such as HOSVD and HOOI can process data tensors in the framework of MICA, there is room for utilizing the nature of the higher-order tensors further effectively. In MICA, the categories in the data represented by the tensor axes are nullified by the matricization treatment. It should be possible to realize tensor ICA processing more meaningfully in such a manner that the data categories represented by the axes remain undestructed for enhanced separation performance.

This paper proposes such a method, namely, higher-order tensor independent component analysis (HOT-ICA), which realizes an effective use of the tensor structure representing data categories such as respective origins of individual data in their physical measurement. Previously, we presented the HOT-ICA concept and its potential by presenting simulation results with rough on-off control of separation-tensor-update sensitivity in HOT-ICA [38]. Here, in this present paper, we describe the details of HOT-ICA with enhanced discussion, and also demonstrate its effectiveness in physical experiments of respiration and heartbeat detection for multiple targets in an environment with obstacles. In addition, we propose a more sophisticated manner of the sensitivity control paying attention to signal-to-noise ratios (SNRs). In the experiments, we compare the results with those of a conventional method, namely, complex-valued frequency-domain ICA (CF-ICA) [13].

This paper is organized as follows. Section II briefly explains the theory of ICA and the Doppler radar. Section III describes HOT-ICA, which is proposed in this paper. Section IV shows the setup and results of numerical experiments including large imbalance in received signals due to obstacle existence in the measurement environment. Section V presents physical experiments with living-human targets to demonstrate the practical effectiveness of the proposed HOT-ICA. Finally, Section VI concludes this paper.

II. Mathematical and Physical Background

A. ICA

A BSS situation is illustrated in Fig. 1 (a). Here we assume an instantaneous mixing process. ICA estimates unmixed original signals based only on received signal information.

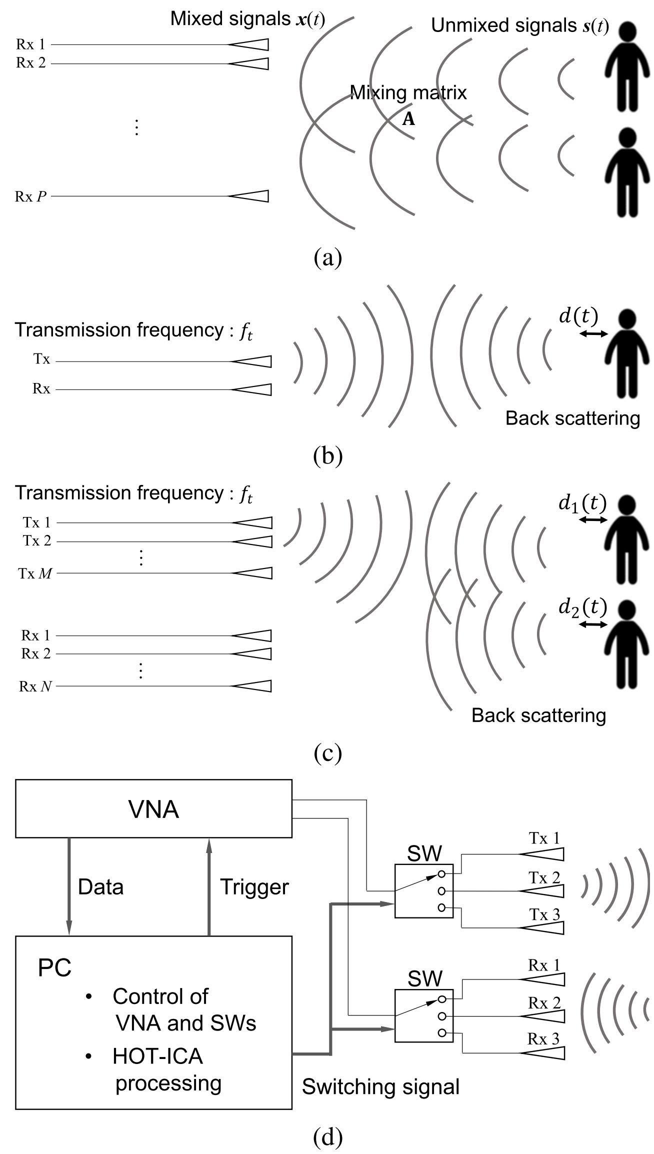

Fig. 1. Conceptual illustrations of (a) general BSS, Doppler radar for (b) single and (c) multiple targets, and (d) the construction of our proposed MIMO radar system (VNA: vector network analyzer, PC: personal computer, SW: switch).

Suppose that P receivers observe mixed signals $\boldsymbol{x}(t) \in \mathbb{C}^{P\times 1}$ originating from independent complex signals $\boldsymbol{s}(t) \in \mathbb{C}^{P\times 1}$. This situation is expressed with a mixing matrix $\mathbf{A} \in \mathbb{C}^{P\times P}$ as

$$\boldsymbol{x}(t) = \mathbf{A}\boldsymbol{s}(t). \quad (1)$$

It is desired to find a separation matrix $\mathbf{B} \in \mathbb{C}^{P\times P}$ that transforms mixed signals $\boldsymbol{x}(t) \equiv [x_1(t) \cdots x_P(t)]^{\mathrm{T}}$ into statistically independent signals $\boldsymbol{y}(t) \equiv [y_1(t) \cdots y_P(t)]^{\mathrm{T}}$, where $[\cdots]^{\mathrm{T}}$ denotes transposition, as

$$\boldsymbol{y}(t) = \mathbf{B}\boldsymbol{x}(t). \quad (2)$$

Each signal in $\boldsymbol{y}(t)$ corresponds to one of the original signals $\boldsymbol{s}(t) \equiv [s_1(t) \cdots s_P(t)]^{\mathrm{T}}$. ICA optimizes the separation matrix $\mathbf{B}$.

Basically, ICA algorithm consists of two parts, namely, whitening and independence maximization. Whitening is a transformation which makes the data uncorrelated with one

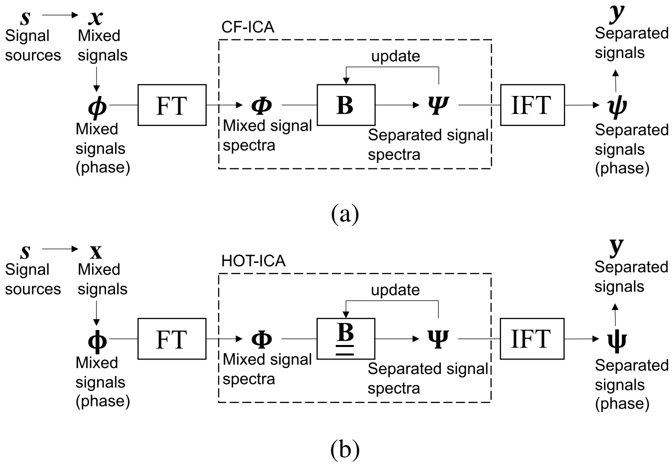

Fig. 2. Processing flow of (a) CF-ICA and (b) HOT-ICA.

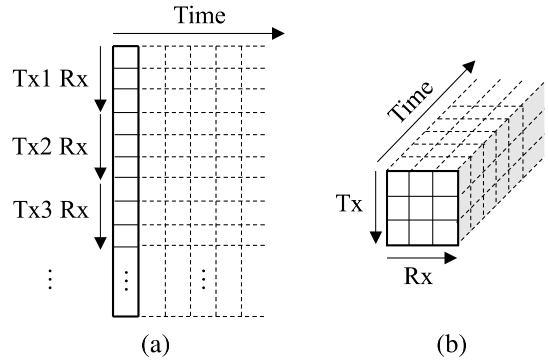

Fig. 3. Structures of signals in (a) conventional ICA processing (e.g. MICA and CF-ICA) and (b) HOT-ICA processing.

another, its mean be 0, and the variance be 1. This process is closely related to principal component analysis (PCA). The independence maximization transforms the uncorrelated data to independent signals. Note that uncorrelatedness mentioned above does not necessarily mean independence. For evaluating independence, nonlinear uncorrelatedness is often used. That is, if arbitrary variables y_1 and y_2 are independent, the following relation holds for arbitrary two nonlinear functions h_1 and h_2:

$$\mathrm{E}\{h_1(y_1)h_2(y_2)\} = \mathrm{E}\{h_1(y_1)\}\mathrm{E}\{h_2(y_2)\}. \tag{3}$$

Thus, we can determine the degree of independence by the degree of satisfaction of (3). In other words, it is estimated that y_1 and y_2 are independent if $h_1(y_1)$ and $h_2(y_2)$ are uncorrelated. In actual algorithms, kurtosis, hyperbolic function such as tanh, or another polynomial is used.

B. Doppler Radar Having a Single Transmitting and Receiving Antennas Respectively

Fig. 1 (b) shows a measurement scene of a Doppler radar. A microwave radiated from transmitting antenna Tx propagates to a target. After backscattered on the body surface, it is received by a receiving antenna Rx. A CW Doppler radar discussed here is a system that detects body surface displacement d caused by respiration and heartbeat.

The phase $\phi(t)$ of the received microwave of frequency f_t is expressed in terms of the target displacement $d(t)$ as

$$\phi(t) \;= 2\pi f_t t + \frac{4\pi d(t)}{\lambda} + \phi_0 \tag{4}$$

where λ and ϕ_0 represent the wavelength and the phase offset, respectively. The displacement is detected as the phase change of the microwave obtained by phase-sensitive detection. Typically, human respiration and heartbeat cause displacement of about 0.5 cm and less than 1 mm, respectively.

III. Proposal of Higher-Order Tensor Independent Component Analysis (HOT-ICA)

Fig. 1 (c) is a conceptual illustration showing a measurement scene of a MIMO Doppler radar to observe multiple targets. First, a microwave radiated from transmitting antenna Tx1 propagates to a target area. Backscattered waves are received by receiving antennas Rx1, $\cdots$, Rxn, $\cdots$, RxN. A next microwave is radiated from transmitting antenna Tx2 and received in the same way. In such a manner, the measurement proceeds with transmitting antennas changed in turn.

Fig. 1 (d) shows the total system construction. The system consists of transmitting and receiving antennas, a vector network analyzer (VNA), switches (SWs), and a personal computer (PC) to control the VNA and the SWs, and to process the obtained data by the proposed HOT-ICA.

HOT-ICA is based on CF-ICA, which processes complex signals in the frequency domain [13]. The processing flow of CF-ICA is shown in Fig. 2 (a). The ICA model described below is independent of the microwave frequency since the relative bandwidth of the microwave CW radar signal is very small in the case of respiration and/or heartbeat measurement. In time-domain ICA, the separation matrix **B** self-organizes for time-series signals that are fed one after another. On the other hand, CF-ICA uses short-time Fourier Transform (STFT) to convert time-domain signals into the frequency domain. It can improve separation performance by limiting the signal frequency band to the minimum containing target signals. Let the mixed signal phase be $\phi_n(t)$ and the separated signal phase be $\psi_i(t)$. The time-domain phase signals $\boldsymbol{\phi}(t) \equiv [\phi_n(t)]$ and $\boldsymbol{\psi}(t) \equiv [\psi_i(t)]$ have time-series STFT spectra expressed as

$$\begin{aligned}\boldsymbol{\Phi}(\omega, t_d) &= [\Phi_n(\omega, t_d)] \\ &= \left[\sum_{\tau=0}^{L_{\mathrm{STFT}}-1} \phi_n(\tau + t_d S)e^{-j\omega\tau}\right],\end{aligned} \tag{5}$$

$$\begin{aligned}\boldsymbol{\Psi}(\omega, t_d) &= [\Psi_i(\omega, t_d)] \\ &= \left[\sum_{\tau=0}^{L_{\mathrm{STFT}}-1} \psi_i(\tau + t_d S)e^{-j\omega\tau}\right]\end{aligned} \tag{6}$$

where L_{STFT} is the length of the Fourier window, S is the moving step of the window, and t_d is the discrete time. After self-organization, an optimized separation matrix **B** works as

$$\boldsymbol{\Psi}(\omega, t_d) = \mathbf{B}(t_d)\boldsymbol{\Phi}(\omega, t_d). \tag{7}$$

In the instantaneous mixing situation, the separation matrix obtained in the frequency domain becomes identical to that in the time domain because of the Fourier-transform (FT) linearity.

The separation algorithm is based on so-called equivariant adaptive separation via independence (EASI) [27]. EASI is a method to simultaneously execute the two ICA processes described in Section II-A, whitening and independence maximization, as a single update process with an updating fraction expressed as

$$\Delta\mathbf{B} = -\mu[\boldsymbol{\Psi}\boldsymbol{\Psi}^{\mathrm{H}} - \mathbf{I} + g(\boldsymbol{\Psi})\boldsymbol{\Psi}^{\mathrm{H}} - \boldsymbol{\Psi}g(\boldsymbol{\Psi})^{\mathrm{H}}]\mathbf{B} \tag{8}$$

where $\boldsymbol{\Psi}^{\mathrm{H}}$ denotes Hermite conjugate of $\boldsymbol{\Psi}$. As mentioned before, $\mathbf{B}$ does not depend on frequency.

Fig. 3 shows structures of mixed signals in general. Conventional methods such as CF-ICA deal with mixed signals in all Txm–(human target)–Rxn channels evenly, as shown in Fig. 3 (a).

Fig. 3 (b) represents the signal structure in HOT-ICA [38]. In contrast to conventional ICA, we construct the framework of HOT-ICA in such a manner that the information represented by the mixed-signal category is undestructed and kept as it is. Then, instead of (7), we express the separation in HOT-ICA by a fourth-order separation tensor $\underline{\underline{\mathbf{B}}}(t_d) \in \mathbb{C}^{p_t\times p_r\times p_t\times p_r}$ for second-order signal tensors $\boldsymbol{\Phi}(\omega, t_d) \in \mathbb{C}^{pt\times pr}$ and $\boldsymbol{\Psi}(\omega, t_d) \in \mathbb{C}^{pt\times pr}$ as

$$\boldsymbol{\Psi}(\omega, t_d) = \underline{\underline{\mathbf{B}}}(t_d)\boldsymbol{\Phi}(\omega, t_d) \tag{9}$$

or, by using elements in the tensors, as

$$\Psi(\omega, t_d)^{(\alpha,\beta)} = \sum_{\gamma=1}^{p_t}\sum_{\delta=1}^{p_r} B(t_d)^{(\alpha,\beta,\gamma,\delta)}\Phi(\omega, t_d)^{(\gamma,\delta)} \tag{10}$$

where α and γ are indices originating from transmitting antennas, while β and δ are related to receiving antennas. We extend the updating formula (8) to HOT-ICA using tensors as

$$\Delta B^{(\alpha,\beta,\gamma,\delta)} = \sum_{\varepsilon=1}^{p_t}\sum_{\zeta=1}^{p_r} W^{(\alpha,\beta,\varepsilon,\zeta)}B^{(\varepsilon,\zeta,\gamma,\delta)} \tag{11}$$

where $\underline{\underline{\mathbf{W}}} = [W^{(\alpha,\beta,\varepsilon,\zeta)}] \in \mathbb{C}^{p_t\times p_r\times p_t\times p_r}$ is an updating weight tensor, and we define it as

$$\begin{aligned} W^{(\alpha,\beta,\gamma,\delta)} = -\mu\Big[&\Psi^{(\alpha,\beta)}\overline{\Psi}^{(\gamma,\delta)} - I^{(\alpha,\beta,\gamma,\delta)} \\ &+g\big(\Psi^{(\alpha,\beta)}\big)\overline{\Psi}^{(\gamma,\delta)} + \Psi^{(\alpha,\beta)}g\Big(\overline{\Psi}^{(\gamma,\delta)}\Big)\Big] \end{aligned} \tag{12}$$

where $\overline{\Psi}$ denotes the conjugate of Ψ. We also define $\underline{\underline{\mathbf{I}}} = [I^{(\alpha,\beta,\gamma,\delta)}] \in \mathbb{C}^{p_t\times p_r\times p_t\times p_r}$ as

$$I^{(\alpha,\beta,\gamma,\delta)} = \begin{cases} 1 & (\alpha = \gamma \cap \beta = \delta), \\ 0 & (\alpha \neq \gamma \cup \beta \neq \delta). \end{cases} \tag{13}$$

When we construct a MIMO system, it is inevitable that respective antennas have various conditions and/or situations different from one another depending on the environment. For example, an amplifier for receiver connected to an antenna may be relatively noisy or defective. In such a case, we should improve the robustness of the overall self-organizing process. This can be achieved by reducing the updating weight associated with the defective channel. HOT-ICA can realize this adjustment as follows. We break down the updating formula (11). By representing updating tensor components related to channels of respective transmitting and receiving antennas Tx1-Rx1, Tx1-Rx2, $\cdots$, Txm-Rxn, $\cdots$, TxM-RxN $(1 \le m \le M), (1 \le n \le N)$ as $\Delta\underline{\underline{\mathbf{B}}}_{\mathrm{Tx1-Rx1}}$, $\Delta\underline{\underline{\mathbf{B}}}_{\mathrm{Tx1-Rx2}}$, $\cdots$, $\Delta\underline{\underline{\mathbf{B}}}_{\mathrm{Tx}m-\mathrm{Rx}n}$, $\cdots$, $\Delta\underline{\underline{\mathbf{B}}}_{\mathrm{Tx}M-\mathrm{Rx}N}$, we can express total update tensor $\Delta\underline{\underline{\mathbf{B}}}$ as

$$\Delta\underline{\underline{\mathbf{B}}} = \Delta\underline{\underline{\mathbf{B}}}_{\mathrm{Tx1-Rx1}} + \Delta\underline{\underline{\mathbf{B}}}_{\mathrm{Tx1-Rx2}} + \cdots + \Delta\underline{\underline{\mathbf{B}}}_{\mathrm{Tx}M-\mathrm{Rx}N} \tag{14}$$

where each $\Delta\underline{\underline{\mathbf{B}}}$ is defined as

$$\Delta B^{(\alpha,\beta,\gamma,\delta)}_{\mathrm{Tx}m-\mathrm{Rx}n} = \sum_{\varepsilon=1}^{p_t}\sum_{\zeta=1}^{p_r} W^{(\alpha,\beta,\varepsilon,\zeta)}_{\mathrm{Tx}m-\mathrm{Rx}n}B^{(\varepsilon,\zeta,\gamma,\delta)}. \tag{15}$$

This representation is possible in HOT-ICA, which keeps tensor axes meaningful. The updating weight tensor $\underline{\underline{\mathbf{W}}}$ is represented as

$$W^{(\alpha,\beta,\varepsilon,\zeta)}_{\mathrm{Tx}m-\mathrm{Rx}n} = \begin{cases} W^{(\alpha,\beta,\varepsilon,\zeta)} & ((\varepsilon = m) \cap (\zeta = n)) \\ 0 & ((\varepsilon \neq m) \cup (\zeta \neq n)). \end{cases} \tag{16}$$

The coefficient $\eta_{\mathrm{Tx}m-\mathrm{Rx}n}$ determines the updating magnitude in self-organization. As an example, in Channel Tx1-Rx1, $\eta_{\mathrm{Tx1-Rx1}}$ $(0 \le \eta_{\mathrm{Tx}m-\mathrm{Rx}n} \le 1)$ is the coefficient for updating $\underline{\underline{\mathbf{W}}}_{\mathrm{Tx1-Rx1}}$. We can obtain a new tensor $\underline{\underline{\mathbf{W}}}'_{\mathrm{Tx}m-\mathrm{Rx}n} \in \mathbb{C}^{p_t\times p_r\times p_t\times p_r}$ having an adjusted updating gain, or sensitivity as

$$\underline{\underline{\mathbf{W}}}'_{\mathrm{Tx}m-\mathrm{Rx}n} = \eta_{\mathrm{Tx}m-\mathrm{Rx}n}\,\underline{\underline{\mathbf{W}}}_{\mathrm{Tx}m-\mathrm{Rx}n}. \tag{17}$$

We describe the details to determine $\eta_{\mathrm{Tx}m-\mathrm{Rx}n}$ in Section IV-B2.

In this way, HOT-ICA can adjust the self-organizing sensitivity for some of the components associated with respective channel situations. This is very effective for measurements employing the MIMO configuration. Conventional methods such as CF-ICA cannot perform this adjustment.

Note that tensor calculation in HOT-ICA is different from that in MICA based on the Tucker decomposition which requires matricization. HOT-ICA keeps the data-tensor structure without nullifying the channel categorization. Hence, HOT-ICA is capable of adaptive signal-source separation every time receiving antennas acquire signals even including possible changes in the measurement environment, resulting in an enhanced robustness. Note also that this proposal is extendable to a processing for n-th order mixed- and unmixed-signal tensors by use of a $2n$-th order separation tensor.

IV. Numerical Experiments

A. Experimental Setup

We conduct numerical experiments by assuming a CW MIMO Doppler radar front-end for signal-source separation based on HOT-ICA. The radar frequency is 2.4 GHz. Fig. 4 shows the placement of antennas and targets. The numbers of transmitting antennas Tx and receiving antennas Rx are $p_t = p_r = 3$, and the number of targets (humans: H) is 4. In HOT-ICA it is not necessary to know the number of original signals in advance. It separates the signals of an upper-limit number, which is identical to the channel

TABLE I
PARAMETERS RELATED TO RESPIRATION AND HEARTBEAT OF EACH TARGET

		Target H1	Target H2	Target H3	Target H4
Respiration	Amplitude [m]	$a_{r_1} = 5.0 \times 10^{-3}$	$a_{r_2} = 5.0 \times 10^{-3}$	$a_{r_3} = 5.0 \times 10^{-3}$	$a_{r_4} = 5.0 \times 10^{-3}$
	Frequency [Hz]	$f_{r_1} = 0.40$	$f_{r_2} = 0.31$	$f_{r_3} = 0.71$	$f_{r_4} = 0.53$
Heartbeat	Amplitude [m]	$a_{h_1} = 5.0 \times 10^{-4}$	$a_{h_2} = 4.0 \times 10^{-4}$	$a_{h_3} = 6.0 \times 10^{-4}$	$a_{h_4} = 3.0 \times 10^{-4}$
	Frequency [Hz]	$f_{h_1} = 1.19$	$f_{h_2} = 1.10$	$f_{h_3} = 1.32$	$f_{h_4} = 1.06$

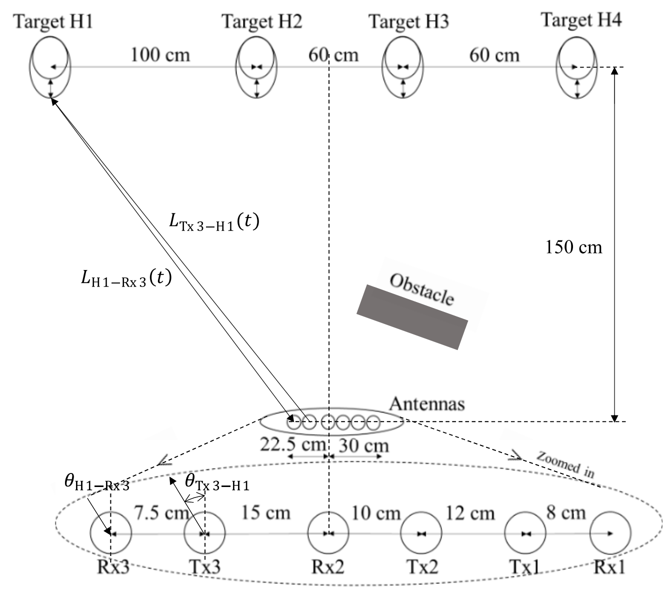

Fig. 4. Placement of transmitting and receiving antennas, Txm and Rxn, and target humans Hk.

number. At the humans, the body moves periodically due to respiration and heartbeat, and the Doppler radar detects the body surface displacement. Then, complex-valued signals are finally obtained. The signals consist of not only the signals originating from the targets but also various noise.

In Fig. 4, an obstacle is placed between targets and antennas. The obstacle has an effect on the received signals. We assume a case that it changes the magnitude of the signals received at antennas Rx1, Rx2, and Rx3 by −3 dB, −1 dB, and 0 dB, respectively.

In the experiments in this section, $\bar{L}_{\mathrm{Tx}m\text{–H}k}$ denotes the average distance from a transmitting antenna Txm $(1 \leqq m \leqq 3)$ to a target Hk $(1 \leqq k \leqq 4)$, and $\bar{L}_{\mathrm{H}k\text{–Rx}n}$ represents that from a target Hk to a receiving antenna Rxn $(1 \leqq n \leqq 3)$. The direction angle from transmitting antenna Txm to target Hk is $\theta_{\mathrm{Tx}m\text{–H}k}$, and the arrival angle from target Hk to receiving antenna Rxn is $\theta_{\mathrm{H}k\text{–Rx}n}$. In the following equations, we use $G_{\mathrm{Tx}m}$ and $G_{\mathrm{Rx}n}$ representing the gains of transmitting and receiving antennas which have same directivity patterns as shown later in Section V, and σ indicating the scattering coefficient of the human body for the electromagnetic waves. The antenna radiation pattern (see Fig. 8 in Section V) and backscattering coefficient (Table II referred to later) were obtained by measurement. Though the value of σ depends on the angle of incidence and scattering, and the human-body

TABLE II
PARAMETERS FOR HOT-ICA AND PROCESSING

Parameter	Value
Sampling rate f_s	11.3 Hz
STFT Window size L_{STFT}	256
Moving step of windows S	2
Frequency band f_{min}–f_{max}	0.095–1.7 Hz
Non-linear function $g(s)$	$\tanh\lvert s\rvert \exp(j \arg(s))$
Learning rate μ	0.0050
Backscattering coefficient σ	0.068
Noise magnitude ρ	$1.0{\times}10^{-4}$

shape is complex and varies among individuals, we treat it roughly as a constant in these numerical experiments.

We determine the original signal model $\boldsymbol{s}(t) \in \mathbb{C}^{4\times 1}$ as

$$\boldsymbol{s}(t) = \begin{bmatrix} s_{\mathrm{H1}}(t) \\ s_{\mathrm{H2}}(t) \\ s_{\mathrm{H3}}(t) \\ s_{\mathrm{H4}}(t) \end{bmatrix} = \begin{bmatrix} \exp(j w_{\mathrm{H1}}(t)) \\ \exp(j w_{\mathrm{H2}}(t)) \\ \exp(j w_{\mathrm{H3}}(t)) \\ \exp(j w_{\mathrm{H4}}(t)) \end{bmatrix} \tag{18}$$

where $w_{\mathrm{H1}}(t)$, $w_{\mathrm{H2}}(t)$, $w_{\mathrm{H3}}(t)$ and $w_{\mathrm{H4}}(t)$ are

$$w_{\mathrm{H1}}(t) = a_{r_1} \sin(2\pi f_{r_1} t) + a_{h_1} \sin(2\pi f_{h_1} t), \tag{19}$$

$$w_{\mathrm{H2}}(t) = a_{r_2} \sin(2\pi f_{r_2} t + \pi/6) + a_{h_2} \sin(2\pi f_{h_2} t + \pi/6), \tag{20}$$

$$w_{\mathrm{H3}}(t) = a_{r_3} \sin(2\pi f_{r_3} t + 3\pi/4) + a_{h_3} \sin(2\pi f_{h_3} t + 3\pi/4), \tag{21}$$

$$w_{\mathrm{H4}}(t) = a_{r_4} \sin(2\pi f_{r_4} t + \pi) + a_{h_4} \sin(2\pi f_{h_4} t + \pi) \tag{22}$$

expressing respiration and heartbeat signals of four humans with their amplitudes and frequencies shown in Table I.

The received signals $\mathbf{E}_{\mathrm{rec}} = [E_{\mathrm{rec}}^{(m,n)}] \in \mathbb{C}^{p_t \times p_r}$ are represented as

$$E_{\mathrm{rec}}(t)^{(m,n)} = \sum_{k=1}^{4} \left[G_{\mathrm{Tx}m} \frac{\exp\left(j 2\pi \frac{L_{\mathrm{Tx}m\text{–H}k}(t)}{\lambda}\right)}{L_{\mathrm{Tx}m\text{–H}k}(t)} \cdot \sigma G_{\mathrm{Rx}n} \frac{\exp\left(j 2\pi \frac{L_{\mathrm{H}k\text{–Rx}n}(t)}{\lambda}\right)}{L_{\mathrm{H}k\text{–Rx}n}(t)} \right] \tag{23}$$

where $L_{\mathrm{Tx}m\text{–H}k}(t)$ and $L_{\mathrm{H}k\text{–Rx}n}(t)$ are written as

$$L_{\mathrm{Tx}m\text{–H}k}(t) = \bar{L}_{\mathrm{Tx}m\text{–H}k} - w_{\mathrm{H}k}(t) \cos\theta_{\mathrm{Tx}m\text{–H}k}, \tag{24}$$

$$L_{\mathrm{H}k\text{–Rx}n}(t) = \bar{L}_{\mathrm{H}k\text{–Rx}n} - w_{\mathrm{H}k}(t) \cos\theta_{\mathrm{H}k\text{–Rx}n}. \tag{25}$$

In the present experiments, the received signals $\mathbf{E}_{\mathrm{rec}}$ and noise $\mathbf{V} = [V^{(m,n)}] \in \mathbb{C}^{p_t \times p_r}$ result in mixed signals $\mathbf{x}(t) = [x(t)^{(\gamma,\delta)}]$ as

$$\mathbf{x}(t) = \mathbf{E}_{\mathrm{rec}}(t) + \rho \mathbf{V} \tag{26}$$

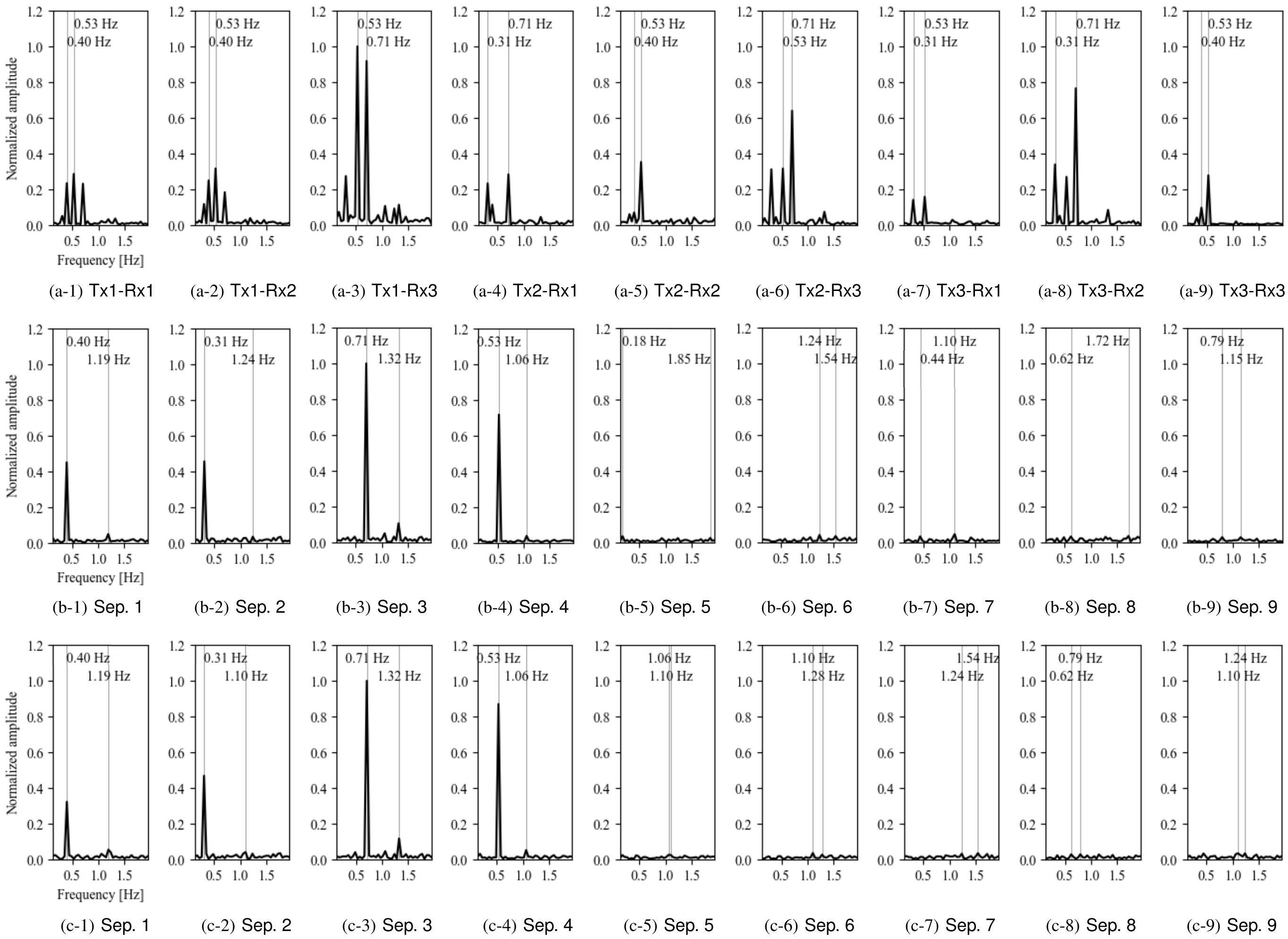

Fig. 5. Spectra of (a-⋆) mixed signals, (b-⋆) signals separated by CF-ICA, and (c-⋆) signals separated by HOT-ICA in the last time window for the setting of three transmitting and three receiving antennas in the environment with an obstacle.

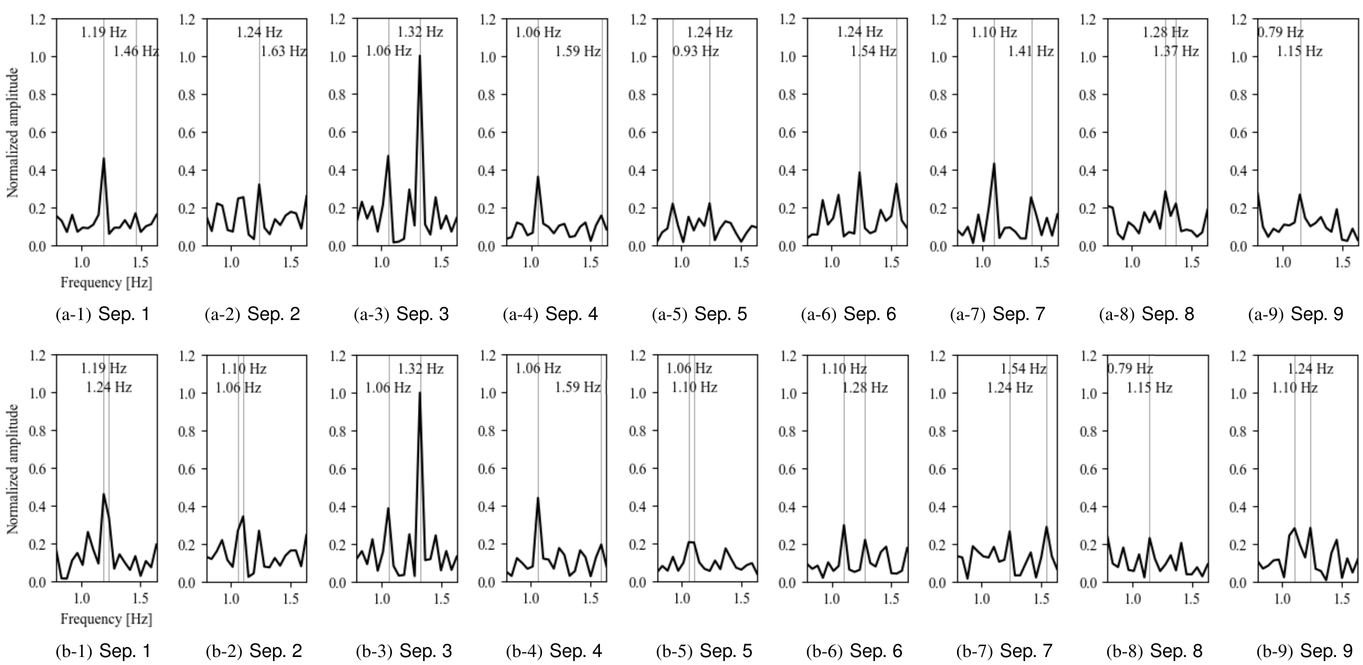

Fig. 6. Heartbeat spectra of (a-⋆) signals separated by CF-ICA and (b-⋆) signals separated by HOT-ICA in the last time window for the setting of three transmitting and three receiving antennas in the environment with an obstacle.

where ρ is noise magnitude and $V^{(m,n)}$ is a noise tensor following the normal distribution with a mean of 0 and a variance of 1.

The parameters of HOT-ICA are shown in Table II. We receive signals for about 177 s. The sampling frequency is $f_s = 11.3$ Hz, and there are 2000 data points. With the STFT of window size $L_{\mathrm{STFT}} = 256$, resulting in a frequency resolution of 0.044 Hz. Moving step is $S = 2$, and the total number of STFT outputs is 872. Then, time index d for the discrete time t_d ranges from $d = 0$ to $D = 871$. In the self-organization, we process signals only in the target frequency band $f_{\min}$–$f_{\max}$ including respiration and heartbeat.

B. Comparison of CF-ICA and HOT-ICA

1) CF-ICA: Figs. 5 (a-$\star$) and (b-$\star$) show the spectra of mixed and separated signals, respectively. The vertical axis represents the signal magnitude normalized in such a way that the maximum signal magnitude in each row becomes unity, and the horizontal axis indicates the frequency. Figs. 5 (a-$\star$) present the mixed signal spectra $\Phi(t_D)$ at the last time window obtained by microwaves transmitted by Tx1 and received by Rx1, denoted as (Tx1, Rx1) as well as those by (Tx1, Rx2), (Tx1, Rx3), (Tx2, Rx1), (Tx2, Rx2), (Tx2, Rx3), (Tx3, Rx1), (Tx3, Rx2), and (Tx3, Rx3) in the order from left to right. These graphs include the original signals scattered by the four targets, the measurement environment, and the sum of the noise at receiving amplifiers.

To make it easier to compare the separation performance of the conventional method (CF-ICA) and the proposed method (HOT-ICA), the spectra including target signals are placed on the left-hand side in Figs. 5 (b-$\star$), (c-$\star$) and Figs. 6 (a-$\star$), (b-$\star$). Thus, the target signals appear in Sep. 1-4 and only noise are in Sep. 5-9. We define an index of rejection ratio $r_{\mathrm{R}} = A_1/A_2$ by using the first peak amplitude A_1 (desired) and the second peak amplitude A_2 (undesired) in each spectrum, and used it to compare the experimental results of the proposed method with those of the conventional method.

In these figures, upper inset frequency values show the frequencies of primary peaks in respective graphs while lower inset values present those of the second peaks. In each of Figs. 5 (b-1), (b-2), (b-3), and (b-4), we can observe a large primary peak in the signal magnitude. The frequencies of the primary peaks correspond to those of respiration of respective targets shown in Table I, and we find that the primary peak represents respiration. Note that a pair of respiration and heartbeat signals of each target appear simultaneously in a single spectrum (see Figs. 5 (b-1), (b-3), and (b-4)). Other spectra in Figs. 5 (b-5)–(b-9) present noise only.

Figs. 6 (a-$\star$) show the spectra of Figs. 5 (b-$\star$) in the heartbeat-frequency band only. In Figs. 6 (a-1), (a-3) and (a-4), the heartbeat signals of targets H1, H3, and H4 are separated, respectively. However, as we can see from Fig. 6 (a-2), the heartbeat signal is not well separated. The primary peak show 1.24 Hz.

2) HOT-ICA: Figs. 5 (c-$\star$) show the results of HOT-ICA, in which we can control updating sensitivity, in the same environment. In this update, we considered that the degree of influence of $\underline{\underline{\mathbf{W}}}_{\mathrm{Tx}m-\mathrm{Rx}n}$ on $\Delta\underline{\underline{\mathbf{B}}}_{\mathrm{Tx}m-\mathrm{Rx}n}$ should be adjusted to be proportional to the reliability of individual received signals, and that the reliability is evaluated as their SNRs. In calculation of a SNR, the signal amplitude in a spectrum is basically determined by the maximum peak height, normalized by the all-spectrum maximum peak height shown in Figs. 5 (a-$\star$), while the noise has almost the same levels for all the spectra. Accordingly, we define the coefficient $\eta_{\mathrm{Tx}m-\mathrm{Rx}n}$ in (17) as the ratio of the magnitude of the peak signal in each Txm-Rxn spectrum to the maximum one in all the spectra. In such a manner, the reduction of desired signals and/or the increase of noise are detectable in the front-end so that the updating sensitivity can be controlled automatically.

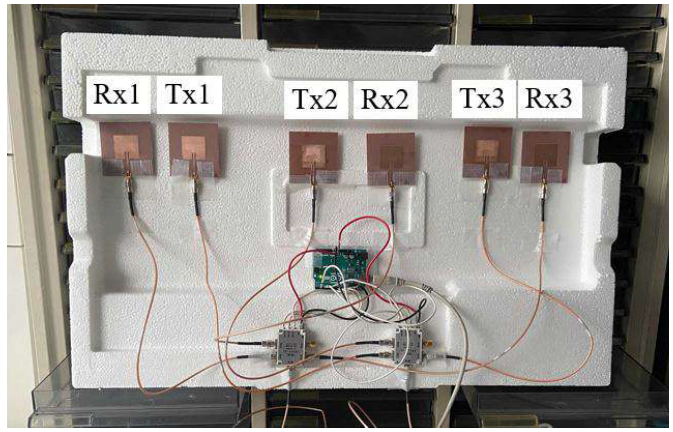

Fig. 7. Antenna array configuration.

In Figs. 6 (b-1)–(b-4), the heartbeat signals of targets H1–H4 are separated, respectively. In contrast with the CF-ICA results in Fig. 6 (a-2), the signal separated by HOT-ICA in Fig. 6 (b-2) has the heartbeat-signal peak of target H2 as the primary one (1.10 Hz) correctly.

The rejection ratios r_{R} of the heartbeat signals separated by using CF-ICA in Figs. 6 (a-1)–(a-4) are 8.72 dB, (failure), 6.55 dB and 7.30 dB, respectively, while those by using HOT-ICA in Figs. 6 (b-1)–(b-4) are 4.97 dB, 2.15 dB, 8.23 dB and 8.04 dB, respectively. Though CF-ICA separates H1 better than HOT-ICA, HOT-ICA separates H2, H3 and H4 better than CF-ICA. We find that the separation performance of HOT-ICA is superior to that of the conventional method.

HOT-ICA can include the sensitivity control to respective components of the updating weight tensor $\underline{\underline{\mathbf{W}}}$. In other words, it realizes direct control of the parameters in the self-organizing dynamics. This successful increase of robustness reveals the significance of keeping the signal categorization in HOT-ICA.

V. Physical Experiments

A. Experimental Setup

We physically perform the experiments described in Section IV with living-human targets and real existence of an obstacle. Fig. 7 is a photo showing the placement of the MIMO antennas. Fig. 8 represents the directivity (gain) of

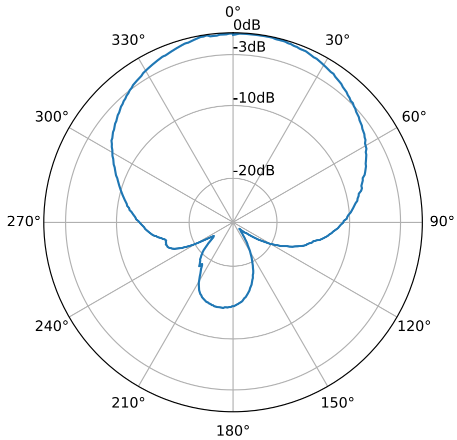

Fig. 8. Directivity (gain) of transmitting and receiving antennas measured at about 1.5 m away corresponding to the following experiments.

Fig. 9. Arrangement of the subjects.

the antennas. We set four targets and arrange them as shown in Fig. 9. The distance from the MIMO antennas to the targets is about 1.5 m. The respiration frequencies of targets H1, H2, H3 and H4 are approximately 0.19 Hz, 0.13 Hz, 0.16 Hz, and 0.10 Hz, respectively. The obstacle is placed 30 cm away from the antenna Rx1 as shown in Fig. 10. The obstacle is aluminum foil, and its size is approximately 25 cm $\times$ 25 cm.

Simultaneously with the observation, we measured the subjects' heartbeat by using contact-type pulse sensors and an oscilloscope. Then, we found that the heartbeat frequencies of targets H1, H2, H3 and H4 are approximately 0.97 Hz, 0.88 Hz, 1.09 Hz, and 0.97 Hz, respectively.

B. Comparison of CF-ICA and HOT-ICA

1) CF-ICA: This section shows the results of CF-ICA processing in the physical experiments. Figs. 11 (a-$\star$), (b-$\star$), and (c-$\star$) represent the mixed-signal spectra $\Phi(t_D)$, spectra separated by CF-ICA $\Psi(t_D)$, and those by HOT-ICA $\Psi(t_D)$, in the same way as that of Figs. 5 in Section IV-B1. In Fig. 11 (a-$\star$), the signals are mixed in all the spectra. In the signal magnitude in Figs. 11 (b-1)–(b-4), we can observe large primary peaks, which are respiration frequencies of targets H1–H4, respectively. They correspond to the actual respiration frequencies.

Spectra shown in Figs. 12 (a-$\star$) include the heartbeat signals separated by CF-ICA. According to Section IV-B1, the heartbeat signal of a target should appear in the same graph as the respiration signal of the same target. That is, Figs. 12 (a-1)–(a-4) represent the heartbeat signals of targets

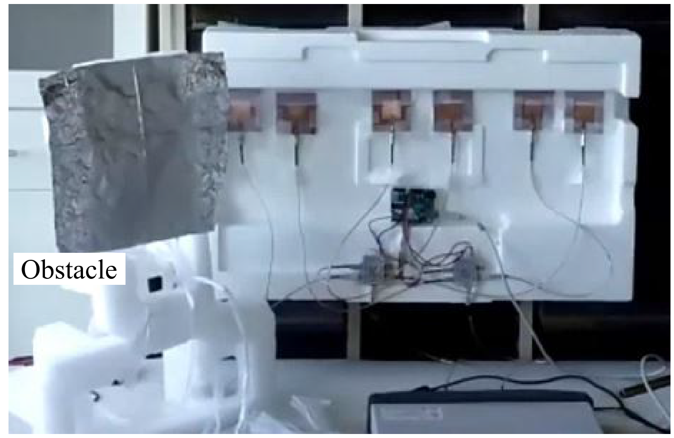

Fig. 10. Obstacle placed in front of the antennas.

H1 (0.97 Hz), H2 (0.88 Hz), H3 (1.09 Hz), and H4 (0.97 Hz), respectively. However, only one signal (H3) coincides with the measurement result obtained by the pulse sensor. In addition, H1, H2, H3 are unseparated. Then, the processing is unsuccessful in total.

2) HOT-ICA: Figs. 11 (c-$\star$) show the results of HOT-ICA with sensitivity control in relation to channels having transmitting and receiving antennas Tx1-Rx1, Tx1-Rx2, $\cdots$, Tx3-Rx3 in the same environment as that in Section V-B1. In the signal magnitude in Figs. 11 (c-1)–(c-4), we can observe large primary peaks, which coincide with the actual respiration frequencies of targets H1, H2, H3, and H4, respectively.

Spectra shown in Figs. 12 (b-$\star$) include the heartbeat signals separated by HOT-ICA. Figs. 12 (b-1)–(b-4) represent the heartbeat signals of targets H1 (0.95 Hz), H2 (0.86 Hz), H3 (0.86 Hz), and H4 (1.33 Hz), respectively. We observed that the heartbeat frequencies for targets H1 and H2 are exactly correct within a resolution unit.

For targets H3 and H4, which are near the obstacle, the heartbeat frequencies are somewhat different from the measurement result of the pulse sensor. The respiration signal originates mainly from abdominal movement, while the heartbeat signal can come from not only the chest but also neck artery, back of the hand, and so on. In addition, the strength of the heartbeat signal is very small. Thus, it is not easy to measure the heartbeat clearly in general. However, our HOT-ICA system is successful in part.

As described above, HOT-ICA is capable of including the control of sensitivity to respective components of the updating weight tensor $\underline{\underline{\mathbf{W}}}$. This operation is realizable only in HOT-ICA because its process reflects the measurement physics, i.e., it preserves the categorization of data unlike the conventional tensor methods. The results of physical experiments showed the significance of HOT-ICA framework.

VI. Conclusion

This paper proposed HOT-ICA. It is a new signal-separation method suitable for categorized data obtained by the measurement for human respiration and heartbeat employing a CW

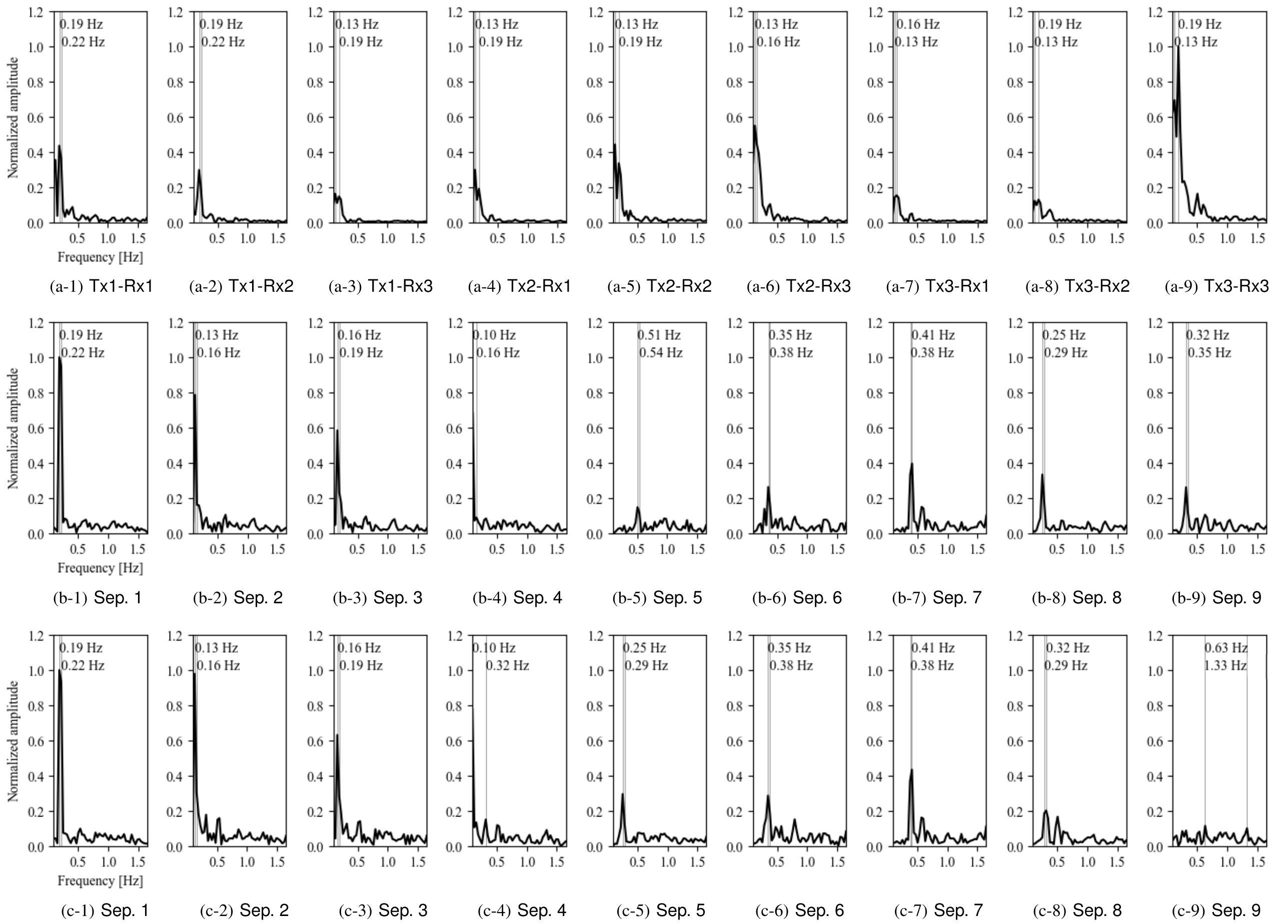

Fig. 11. Spectra of (a-⋆) mixed signals, (b-⋆) signals separated by CF-ICA, and (c-⋆) signals separated by HOT-ICA in the last time window for the setting of three transmitting and three receiving antennas in the environment with an obstacle.

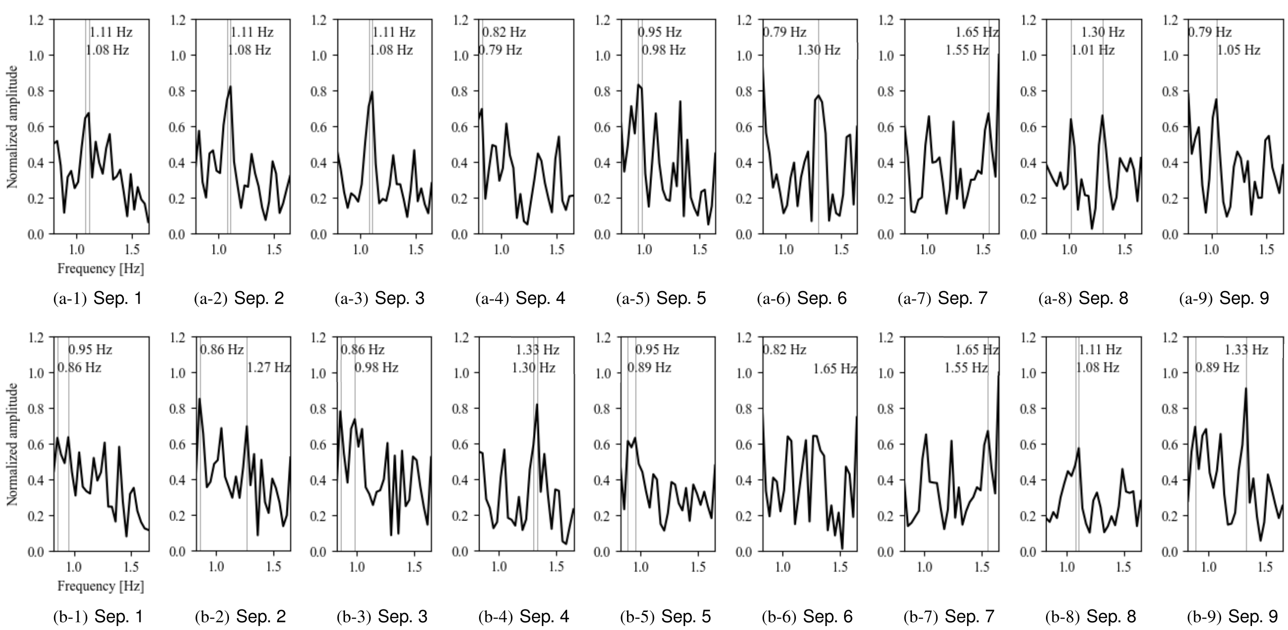

Fig. 12. Heartbeat spectra of (a-⋆) signals separated by CF-ICA and (b-⋆) signals separated by HOT-ICA in the last time window for the setting of three transmitting and three receiving antennas in the environment with an obstacle.

MIMO Doppler radar, where the physical Tx or Rx in the measurement corresponds to each axis of the tensor. We conducted numerical experiments as well as physical experiments. We set an obstacle in the measurement environment, which causes the attenuation of target signals and the decrease of SNR, and compared the separation performances of proposed HOT-ICA with conventional CF-ICA. As a result, we found that HOT-ICA is more robust to the obstacle existence than conventional CF-ICA, leading to more flexible observation in various measurement situations. This robustness is achieved by HOT-ICA's signal processing dynamics that preserves the categories in the data to realize more powerful self-organization ability.

Acknowledgment

The authors would like to thank Takahiro Nakanishi, Ryogo Saito, Junya Kato, Ryuta Imai, Bungo Konishi, Lena Azuma, Ryotaro Yamakawa, and Yanqi Zhu of The University of Tokyo for their help in the experiments.

References

[1] J. C. Lin, "Noninvasive microwave measurement of respiration," *Proc. IEEE*, vol. 63, no. 10, p. 1530, Oct. 1975.

[2] C. Li, Y. Xiao, and J. Lin, "Experiment and spectral analysis of a low-power Ka-band heartbeat detector measuring from four sides of a human body," *IEEE Trans. Microw. Theory Techn.*, vol. 54, no. 12, pp. 4464–4471, Dec. 2006.

[3] C. Li and J. Lin, "Random body movement cancellation in Doppler radar vital sign detection," *IEEE Trans. Microw. Theory Techn.*, vol. 56, no. 12, pp. 3143–3152, Dec. 2008.

[4] C. Gu, C. Li, J. Lin, J. Long, J. Huangfu, and L. Ran, "Instrument-based noncontact Doppler radar vital sign detection system using heterodyne digital quadrature demodulation architecture," *IEEE Trans. Instrum. Meas.*, vol. 59, no. 6, pp. 1580–1588, Jun. 2010.

[5] M.-C. Huang, J. J. Liu, W. Xu, C. Gu, C. Li, and M. Sarrafzadeh, "A self-calibrating radar sensor system for measuring vital signs," *IEEE Trans. Biomed. Circuits Syst.*, vol. 10, no. 2, pp. 352–363, Apr. 2016.

[6] G. Cerasuolo, O. Petrella, L. Marciano, F. Soldovieri, and G. Gennarelli, "Metrological characterization for vital sign detection by a bioradar," *Remote Sens.*, vol. 9, no. 10, p. 996, Sep. 2017. [Online]. Available: https://www.mdpi.com/2072-4292/9/10/996

[7] Y. Lee et al., "A novel non-contact heart rate monitor using impulse-radio ultra-wideband (IR-UWB) radar technology," *Sci. Rep.*, vol. 8, no. 1, p. 13053, 2018.

[8] K.-M. Chen, Y. Huang, J. Zhang, and A. Norman, "Microwave life-detection systems for searching human subjects under earthquake rubble or behind barrier," *IEEE Trans. Biomed. Eng.*, vol. 47, no. 1, pp. 105–114, Jan. 2000.

[9] I. Arai, "Survivor search radar system for persons trapped under earthquake rubble," in *Proc. Asia–Pacific Microw. Conf. (APMC)*, vol. 2, Dec. 2001, pp. 663–668.

[10] K. Wang, Z. Zeng, and J. Sun, "Through-wall detection of the moving paths and vital signs of human beings," *IEEE Geosci. Remote Sens. Lett.*, vol. 16, no. 5, pp. 717–721, May 2019.

[11] M. Donelli, "A rescue radar system for the detection of victims trapped under rubble based on the independent component analysis algorithm," *Prog. Electromagn. Res. M*, vol. 19, pp. 173–181, 2011.

[12] A. E. Bezer and A. Hirose, "Proposal of a human heartbeat detection/monitoring system employing chirp Z-transform and time-sequential neural prediction," in *Proc. Int. Conf. Neural Inf. Process. (ICONIP)*, Kyoto, Japan. Heidelberg, Germany: Springer, 2016, pp. 510–516.

[13] T. Nakanishi and A. Hirose, "Proposal of adaptive Search-and-Rescue radar system with online complex-valued frequency-domain independent component analysis," in *Proc. IEEE Int. Geosci. Remote Sens. Symp. (IGARSS)*, Jul. 2019, pp. 9431–9434.

[14] Analog Devices. *miRadar 8: 24 GHz FMCW MIMO Radar Platform by Sakura Tech*. Accessed: Jan. 2021. [Online]. Available: https://www.analog.com/en/education/education-library/videos/5557613174001.html

[15] M. Ambrosanio, S. Franceschini, G. Grassini, and F. Baselice, "A multichannel ultrasound system for non-contact heart rate monitoring," *IEEE Sensors J.*, vol. 20, no. 4, pp. 2064–2074, Feb. 2020.

[16] T. Sakamoto, P. J. Aubry, S. Okumura, H. Taki, T. Sato, and A. G. Yarovoy, "Noncontact measurement of the instantaneous heart rate in a multi-person scenario using X-band array radar and adaptive array processing," *IEEE J. Emerg. Sel. Topics Circuits Syst.*, vol. 8, no. 2, pp. 280–293, Jun. 2018.

[17] J. Hérault and B. Ans, "Circuits neuronaux á synapses modifiables: Décodage de messages composites par apprentissage non supervisé," *Comp. Rendus de l'Académie des Sci.*, vol. 299, pp. 525–528, Mar. 1984.

[18] C. Jutten and A. Taleb, "Source separation: From dusk till dawn," in *Proc. 2nd Int. Workshop Independ. Compon. Anal. Blind Source Separat. (ICA)*, 2000, pp. 15–26.

[19] A. Hyvärinen, J. Karhunen, and E. Oja, *Independent Component Analysis (Adaptive and Cognitive Dynamic Systems: Signal Processing, Learning, Communications and Control)*. Hoboken, NJ, USA: Wiley, 2001.

[20] S. Ikeda and N. Murata, "A method of ICA in time-frequency domain," in *Proc. Int. Workshop Independ. Compon. Anal. Eng. Blind Signal Separat. (ICA)*, Aussois, France, Jan. 1999, pp. 365–371.

[21] H. Sawada, R. Mukai, S. Araki, and S. Makino, "Polar coordinate based nonlinear function for frequency-domain blind source separation," in *Proc. IEEE Int. Conf. Acoust. Speech Signal Process.*, vol. 1, May 2002, pp. I-1001–I-1004.

[22] H. Sawada, R. Mukai, S. Araki, and S. Makino, "A robust and precise method for solving the permutation problem of frequency-domain blind source separation," *IEEE Trans. Speech Audio Process.*, vol. 12, no. 5, pp. 530–538, Sep. 2004.

[23] A. Hirose, *Complex-Valued Neural Networks* (Studies in Computational Intelligence). Berlin, Germany: Springer, 2012.

[24] A. Hirose and S. Yoshida, "Generalization characteristics of complex-valued feedforward neural networks in relation to signal coherence," *IEEE Trans. Neural Netw. Learn. Syst.*, vol. 23, no. 4, pp. 541–551, Apr. 2012.

[25] A. Hirose and R. Eckmiller, "Behavior control of coherent-type neural networks by carrier-frequency modulation," *IEEE Trans. Neural Netw.*, vol. 7, no. 4, pp. 1032–1034, Jul. 1996.

[26] A. Cichocki, R. Unbehauen, and E. Rummert, "Robust learning algorithm for blind separation of signals," *Electron. Lett.*, vol. 30, no. 17, pp. 1386–1387, 1994.

[27] J. F. Cardoso and B. H. Laheld, "Equivariant adaptive source separation," *IEEE Trans. Signal Procces.*, vol. 44, no. 12, pp. 3017–3030, Dec. 1996.

[28] A. O. Vasilescu and D. Terzopoulos, "Multilinear independent components analysis," in *Proc. IEEE Comput. Soc. Conf. Comput. Vis. Pattern Recognit. (CVPR)*, vol. 1, Jun. 2005, pp. 547–553.

[29] M. A. O. Vasilescu and D. Terzopoulos, "Multilinear (tensor) image synthesis, analysis, and recognition [exploratory DSP]," *IEEE Signal Process. Mag.*, vol. 24, no. 6, pp. 118–123, Nov. 2007.

[30] B. N. Sheehan and Y. Saad, "Higher order orthogonal iteration of tensors (HOOI) and its relation to PCA and GLRAM," in *Proc. SIAM Int. Conf. Data Mining*, Minneapolis, MN, USA, Apr. 2007, pp. 355–365.

[31] T. G. Kolda and B. W. Bader, "Tensor decompositions and applications," *SIAM Rev.*, vol. 51, no. 3, pp. 455–500, Sep. 2009.

[32] A. H. Phan and A. Cichocki, "Tensor decompositions for feature extraction and classification of high dimensional datasets," *IEICE Nonlinear Theory Appl.*, vol. 1, no. 1, pp. 37–68, 2010.

[33] L. R. Tucker, "Some mathematical notes on three-mode factor analysis," *Psychometrika*, vol. 31, no. 3, pp. 279–311, 1966.

[34] Y. Li and A. Ngom, "Nonnegative least-squares methods for the classification of high-dimensional biological data," *IEEE/ACM Trans. Comput. Biol. Bioinf.*, vol. 10, no. 2, pp. 447–456, Mar./Apr. 2013.

[35] D. Ai, G. Duan, X. Han, and Y.-W. Chen, "Generalized N-dimensional independent component analysis and its application to multiple feature selection and fusion for image classification," *Neurocomputing*, vol. 103, pp. 186–197, Mar. 2013.

[36] T. Fukuta, T. Yoshikawa, and T. Furuhashi, "A study on feature extraction and discrimination of P300 wave based on ICA," in *Proc. Fuzzy Syst. Symp.*, vol. 31, 2015, pp. 729–732.

[37] G. Zhou, Q. Zhao, Y. Zhang, T. Adalí, S. Xie, and A. Cichocki, "Linked component analysis from matrices to high-order tensors: Applications to biomedical data," *Proc. IEEE*, vol. 104, no. 2, pp. 310–331, Feb. 2016.

[38] S. Goto, R. Natsuaki, and A. Hirose, "Proposal of higher-order tensor independent component analysis for signal separation in multiple-input multiple-output respiration/heartbeat remote sensing," in *Proc. 43rd Annu. Int. Conf. IEEE Eng. Med. Biol. Soc. (EMBC)*, Nov. 2021, pp. 325–328.

Seishiro Goto (Graduate Student Member, IEEE) received the B.Eng. degree in mechanical engineering informatics from Meiji University, Kanagawa, Japan, in 2019, and the M.Eng. degree in bioengineering from The University of Tokyo, Tokyo, Japan, in 2021, where he is currently pursuing the Ph.D. degree.

His current research interests include remote sensing systems and signal processing. He received Young Researcher Award, IEEE Computational Intelligence Society (CIS) Japan Chapter, in 2022.

Ryo Natsuaki (Senior Member, IEEE) received the B.S., M.S., and Ph.D. degrees in electrical engineering from The University of Tokyo, Japan, in 2009, 2011, and 2014, respectively.

He was an Aerospace Project Research Associate with the Japan Aerospace Exploration Agency (JAXA), Tsukuba, Japan, from 2014 to 2017. He was also a Guest Scientist with the Microwaves and Radar Institute, German Aerospace Center (DLR), Oberpfaffenhofen, Germany, from 2018 to 2020, under the JSPS Overseas Research Fellowships. He is currently an Associate Professor with the Department of Electrical Engineering and Information Systems, The University of Tokyo. His research interests include active remote sensing with synthetic aperture radar (SAR).

Dr. Natsuaki is a member of the Institute of Electronics, Information and Communication Engineers (IEICE), Japan, and the American Geophysical Union (AGU). He is also a Technical Committee Member of the Frequency Allocations in Remote Sensing (FARS) Technical Committee and the Remote Sensing Environment, Analysis and Climate Technologies Technical Committee (REACT) in GRSS. He was the Publicity Chair of the IEEE International Geoscience and Remote Sensing Symposium (IGARSS) 2019. He also serves as an Associate Editor for IEEE TRANSACTIONS ON GEOSCIENCE AND REMOTE SENSING and the Secretary for the IEICE Technical Committee on Electromagnetic Theory (EMT). He was the Secretary of the IEEE GRSS Japan Chapter from 2014 to 2017 and the IEICE Technical Committee on Space, Aeronautical and Navigational Electronics (SANE) from 2017 to 2022.

Akira Hirose (Fellow, IEEE) received the Ph.D. degree in electronic engineering from The University of Tokyo, Tokyo, Japan, in 1991.

In 1987, he joined the Research Center for Advanced Science and Technology (RCAST), The University of Tokyo, as a Research Associate. In 1991, he was appointed as an Instructor with RCAST. From 1993 to 1995, on leave of absence from The University of Tokyo, he joined the Institute for Neuroinformatics, University of Bonn, Bonn, Germany. He is currently a Professor with the Department of Electrical Engineering and Information Systems, The University of Tokyo. His research interests include wireless electronics and neural networks, in which he has published several books, such as *Complex-Valued Neural Networks* (2nd edition, 2012).

Dr. Hirose is a fellow of the Institute of Electronics, Information and Communication Engineers (IEICE) and a member of the Japanese Neural Network Society (JNNS) and the Asia–Pacific Neural Network Society (APNNS). He has been a member of the IEEE Computational Intelligence Society (CIS) Neural Networks Technical Committee (NNTC) since 2009 and a Governing Board Member of the Asia–Pacific Neural Network Assembly (APNNA)/APNNS since 2006. He was the IEEE Geoscience and Remote Sensing Society (GRSS) All Japan Chapter Chair from 2013 to 2015, the IEEE CIS All Japan Chapter Chair from 2017 to 2018, and also the General Chair of the Asia–Pacific Conference on Synthetic Aperture Radar (APSAR) 2013 Tsukuba, the International Conference on Neural Information Processing (ICONIP) 2016 Kyoto, and the International Geoscience and Remote Sensing Symposium (IGARSS) 2019 Yokohama. He will be the General Co-Chair of the IEEE World Congress on Computational Intelligence (WCCI) 2024 Yokohama. He has been the Founding Chair of the NNTC Complex-Valued Neural Network Task Force since 2010. He was the President of APNNS in 2016, the President of JNNS from 2013 to 2015, and the Vice President of the IEICE Electronics Society (ES) from 2013 to 2015. He was the Editor-in-Chief of the *IEICE Transactions on Electronics* from 2011 to 2012. He served as an Associate Editor for journals, such as IEEE TRANSACTIONS ON NEURAL NETWORKS from 2009 to 2011 and *IEEE Geoscience and Remote Sensing Newsletter* from 2009 to 2012. He has been serving as an Associate Editor for IEEE TRANSACTIONS ON NEURAL NETWORKS AND LEARNING SYSTEMS since 2020.